Optics Letters

# Evanescent field refractometry in planar optical fiber

Christopher Holmes,* Alexander Jantzen, Alan C. Gray, Paul C. Gow, Lewis G. Carpenter, Rex H. S. Bannerman, James C. Gates, and Peter G. R. Smith

*Optoelectronics Research Centre, University of Southampton, Mountbatten Building, Salisbury Road, Southampton SO17 1BJ, UK*
**Corresponding author: christopher.holmes@soton.ac.uk*

*Received 25 October 2017; revised 1 December 2017; accepted 1 December 2017; posted 6 December 2017 (Doc. ID 309889); published 9 February 2018*

**This Letter demonstrates a refractometer in integrated optical fiber, a new optical platform that planarizes fiber using flame hydrolysis deposition (FHD). The unique advantage of the technology is survivability in harsh environments. The platform is mechanically robust, and can survive elevated temperatures approaching 1000°C and exposure to common solvents, including acetone, gasoline, and methanol. For the demonstrated refractometer, fabrication was achieved through wet etching an SMF-28 fiber to a diameter of 8 μm before FHD planarization. An external refractive index was monitored using fiber Bragg gratings (FBGs), written into the core of the planarized fiber. A direct comparison to alternative FBG refractometers is made, for which the developed platform is shown to have comparable sensitivity, with the added advantage of survivability in harsh environments.**



***OCIS codes:*** (060.3735) Fiber Bragg gratings; (060.2370) Fiber optics sensors; (230.7390) Waveguides, planar.

https://doi.org/10.1364/OL.43.000791

Optical monitoring in environmental extremes is an important research area, as it can provide parameter information that would otherwise be difficult to access electronically. Sensors based on optical fiber, in particular, have proven to be attractive [1,2] namely because they do not pose a spark risk in flammable environments, have immunity to electromagnetic interference, are resilient at elevated temperatures (over 100°C), and have the ability to form part of a large distributed network. This Letter reports on a new passive planar optical platform termed integrated optical fiber (IOF). Its key advantage is the ability for it to be deployed in even harsher environmental conditions. It possesses the optical advantages associated with fiber, while enabling a basis for planar functionality. The IOF platform, illustrated in Fig. 1, is composed of an optical fiber bound to a planar substrate through use of flame hydrolysis deposition (FHD). The FHD glass forms a miscible alloy between the planar carrier substrate (silicon) and the fiber during a high temperature (>1000°C) consolidation phase. There is no use of glues or epoxy. As such, the platform can be taken up to elevated temperatures approaching that used in its consolidation. It can also endure exposure to common solvents (e.g., acetone, methanol, and gasoline) with no notable degradation. Since FHD glass is of optical quality, it is also suitable for direct optical interaction. Furthermore, optical fiber can transition on and off chip, as illustrated in Fig. 1(b). This monolithic coupling feature further removes the requirement for glues and epoxy that are typically used to secure an optical fiber when coupling to a planar chip [3]. Thus, the mechanical weakness brought about by these mechanisms of binding is also removed.

Developments in IOF have thus far been limited to utilizing the environmental stability [4] and/or physical robustness [5,6] of the platform. To the best of our knowledge, this Letter is the first to report direct optical interaction between the fiber core and the FHD binding medium. In this demonstration, the evanescent field of the planarized fiber is exposed and a Bragg grating used to infer external refractive index. It is noted the Bragg wavelength, $\lambda_B$, is dependent on the effective refractive index, $n_{\text{eff}}$, relating to the periodicity of the grating, $\Lambda$:

$$\lambda_B = 2\Lambda n_{\text{eff}}. \quad (1)$$

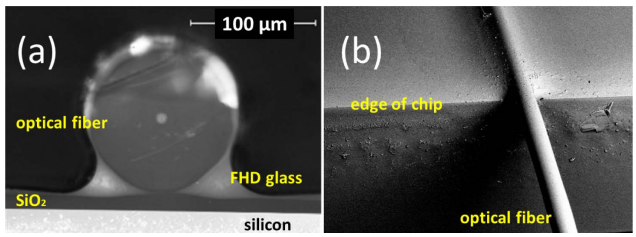


**Fig. 1.** (a) Cross-sectional profile of an IOF and (b) demonstration of off-chip/on-chip routing. (For scale, the optical fiber shown is an unetched SMF-28 with 125 μm diameter.)

FBGs have the distinct advantage of multi-parameter multiplexed sensing capability [7], which includes the ability to monitor temperature, strain, and external refractive index [8].

Work by this group has previously commercialized planar-Bragg grating refractometers, for Biopharma applications [9,10], achieving spectral sensitivities of 190 nm/refractive index units (RIUs) and corresponding index resolutions of $2 \times 10^{-6}$ RIU [3]. Other notable refractometer configurations include those that harness surface plasmon resonances [11] and those that utilize microstructured fiber [12–14]. These typically have an order of magnitude increased RIU resolution, but do not have the multiplexing capability associated with fiber Bragg gratings (FBGs). There are also several reported approaches that expose the evanescent field of an optical fiber and interrogate with long or short period gratings. These approaches couple light from a guided core to cladding modes through use of tapers [15], tilted Bragg gratings [16–18], and long period gratings [19]. Surface plasmon interactions can also be used in combination with these to enhance sensitivity [11,20]. Due to bandwidth efficiency (and, thus, the potential for greater parameter monitoring), this Letter considers guided core mode confinement only. For this, two principle geometries exist: side access [8,21] and uniform access [22], illustrated in Fig. 2. Side access is achieved by potting the fiber into an epoxy and machining it via lapping and polishing. Uniform access uses an etchant, typically buffered hydrofluoric acid, to uniformly wet etch the silica-clad material. While both these approaches have been proven, they have limitations when exposed to certain environments, including certain common solvents, turbulent flows, or high temperatures (in excess 300°C). Upon exposure to these environments, they exhibit an inherent fragility.

This Letter builds largely on the concept of thinned fiber Bragg gratings (thFBGs) [15,22], which is a uniform access geometry. It is argued that since a greater proportion of the evanescent field can be exposed, an enhanced sensitivity can be attained, compared to a side access approach of a comparable effective fiber diameter, $d$. However, as a result of the fiber's small diameter (<10 μm), the geometry is mechanically more fragile, e.g., to turbulent flows. This Letter planarizes and ruggedizes the thFBG concept, with minimal compromise to sensitivity using an IOF geometry, illustrated in Fig. 2.

Design considerations for thinned IOF need to ensure that waveguiding is still maintained. As such, a 15 μm oxide layer is required between the fiber and silicon, as shown in Fig. 2. The purpose of the oxide is to act as an optical buffer, so that light does not leak into the underlying silicon substrate. Another design consideration is the refractive index and thickness of the FHD layer. This must be tailored such that light does not couple out from the core into the features immediately beneath the fiber that resemble a frozen-in meniscus, termed and labeled in Fig. 2 as wings. To understand how fabrication variables influence sensitivity, a commercial mode solver (FIMMWAVE by Photon Design) was used. In these computer simulations the diameter of the fiber is set to 9 μm, the core diameter to 8 μm, and the cross-sectional area of wings as 3 $\mu m^2$. The first parameter considered was wing refractive index contrast, $\Delta n$, defined relative to the thermally grown oxide (assumed to be 1.4452 at 1550 nm wavelength). Figure 3 shows the simulated sensitivity for this parameter around an external refractive index of 1.444, a refractive index region of particular interest for automobile and aviation fuel monitoring [23]. It is evident from this simulation that the lower the refractive index of the wings the greater the spectral sensitivity. This response is understood through modal confinement. As the refractive index of the wings increase, an increasing fraction of the modal power is supported in and near their proximity, reducing external fractional power and thus sensitivity. Modal confinement is illustrated in the insets of Fig. 3 for the two extremities of the simulation.

The refractive index of the fiber core was also considered in the simulations. This parameter can be manipulated through ultraviolet (UV) exposure; feasibly, this can be of the order $2 \times 10^{-2}$. Figure 4 shows the response to this parameter as the refractive index of the core increases. As the inserted modal solutions depict increased, modal confinement in the core occurs for high core refractive indices, thus reducing sensitivity.

To test the theoretical models, a demonstrator was fabricated and calibrated using Cargille refractive index oils (Cargille Labs, series AAA and AA). Fabrication involved mechanically stripping the acrylate coating from an SMF-28 optical fiber before wet etching it in a buffered hydrofluoric acid (HF) solution (29% concentrated). Etching was periodically monitored using an optical microscope, and an etch rate of 0.53 $\mu m \cdot min^{-1}$ was inferred. At a diameter of 8 μm, the wet etch was ceased, and the fiber was layered onto a silicon wafer, with a 15 μm pre-grown oxide. To form IOF, an adapted FHD process was used [5]. The deposition passed chloride-based pre-cursors of $SiCl_4$ at 137 sccm, $PCl_3$ at 31 sccm, and $BCl_3$ at 69 sccm through an argon sheathed oxy-hydrogen flame with flow rates of 8.0 $l \cdot min^{-1}$, 6.5 $l \cdot min^{-1}$, and 1.9 $l \cdot min^{-1}$ for

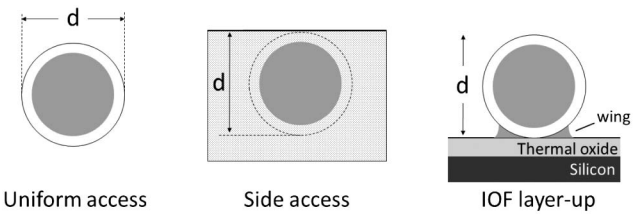


**Fig. 2.** Cross sections of the evanescent field exposed core in a uniform access, side access, and IOF layer-up geometry, respectively.

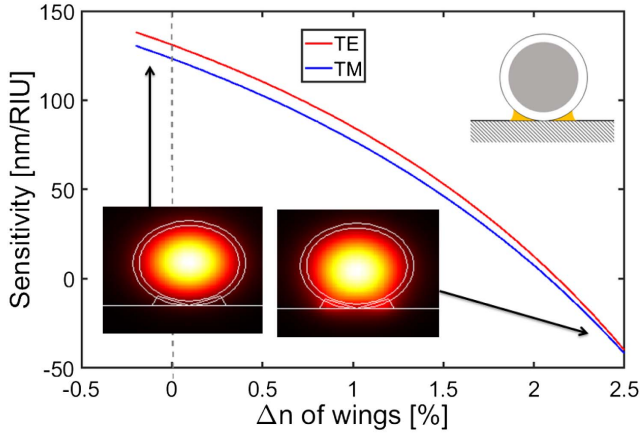


**Fig. 3.** Finite element method simulation considering the sensitivity dependence subject to the refractive index of the IOF wings (highlighted in yellow within the inset) around an external refractive index of 1.444. The modal power distribution is shown in the insets.

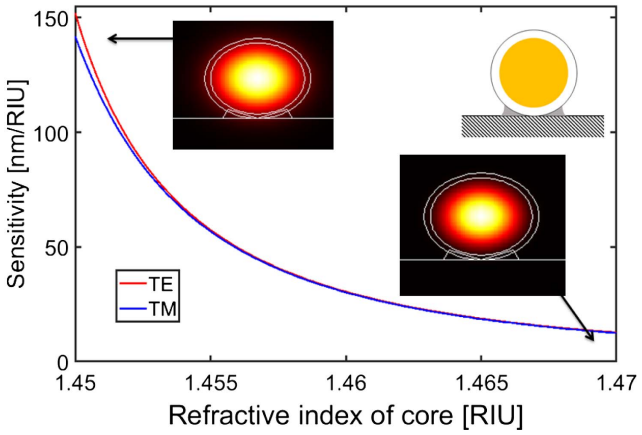


**Fig. 4.** Finite element method simulation considering the sensitivity dependence subject to the refractive index of the core (highlighted in yellow within the inset) around an external refractive index of 1.444. The modal power distribution is shown in the insets.

Ar, $H_2$, and $O_2$, respectively. The FHD soot produced was subsequently consolidated at a temperature of 1250°C in a helium flow atmosphere of 1.90 $l \cdot min^{-1}$. Through scanning electron microscopy (SEM) imaging of the cross section of the device was estimated to have an FHD infill below the fiber (wings) of 3 $\mu m^2$, shown in Fig. 5 inset. The borophosphosilicate deposited glass had a measured refractive index comparable to that of the thermally grown oxide (1.4452 ± 0.0001 at 1553 nm wavelength) calibrated using a prism coupler technique (Metricon). The nominal thickness of the deposited FHD layer was 0.5 μm. This was characteristically thicker for the wing features as a meniscus forms during the consolidation phase.

Surface roughness of the optical fiber was measured using a white light interferometer (ZeScope, Zemetrics). Immediately after HF etching fiber roughness was measured to be 62.2 nm (Sa) and after FHD processing, this was reduced to only 9.1 nm (Sa). From analytical theory, it is understood that propagation loss scales to the square-root of surface roughness [24]. Therefore, it is expected that a reduction in propagation loss will follow FHD processing. Quantification of this is considered beyond the scope of this Letter, but will be the subject of future investigation.

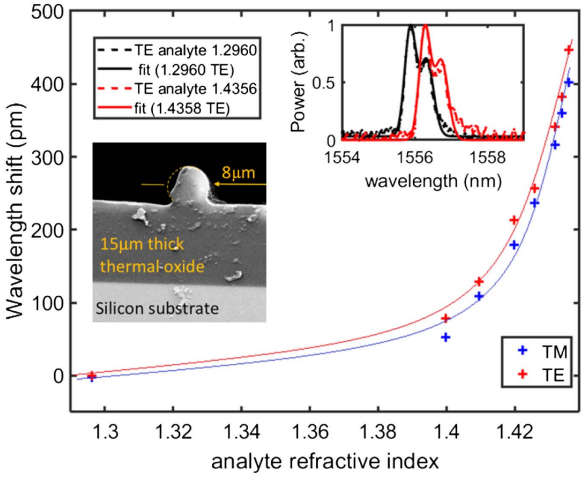


**Fig. 5.** External refractive index sensitivity of an IOF chip for both TE and TM polarizations. The insets show the spectral TM back reflection for two external refractive indices (1.296 and 1.436) and an SEM cross section of the device.

Bragg gratings were written into the fiber using a direct UV writing (DUW) process [10]. This technique uses two coherent UV (continuous-wave 244 nm) beams, focused and overlapping with a spot size of approximately 7 μm in diameter. To enhance the photosensitivity of the fiber, the device was hydrogenated in a high pressure (120 bar) hydrogen atmosphere for seven days. The writing conditions used a fluence of 30 $kJ \cdot cm^{-2}$, a grating length 4 mm, a period of 534.0 nm, and a Gaussian apodized windowing function upon the grating. Systematic linear birefringence resulted in two well-defined polarization modes that propagate through the attached fiber, with very distinct phase velocities. These were selectively launched through a butt-coupled polarization maintaining fiber. The resulting reflection spectrum from the grating is presented in the inset of Fig. 5. From Eq. (1), and taking the Bragg wavelength, $\lambda_B$, as 1556.054 nm, an effective refractive index, $n_{\text{eff}}$, of 1.45698 is inferred when the device is surrounded by air. The spectral asymmetry observed in the Fig. 5 inset is likely due to misalignment in the UV writing process between the small writing spot (7 μm) and the core of the fiber (8 μm). This is either inherent misalignment of the writing process or the fiber not being layered up straight over the grating length; both of these issues are to be addressed in future generations of the device.

Characterization of sensitivity to external refractive index was made, and is illustrated in Fig. 5. A double Gaussian function, with constant relative offsets and amplitudes was used to fit transverse electric (TE)- and transverse magnetic (TM)-polarized launches, respectively. Between refractive index oils, the sample underwent two cleaning procedures with acetone, removing fluid between procedures with the use of a nitrogen gun.

For external refractive indices around 1.435, the spectral sensitivity is 32 nm/RIU. To compare this level of sensitivity with the two other geometrical approaches outlined in Fig. 2, empirical data were extracted from the literature [22,25], and simulations were made, illustrated in Fig. 6. The simulated spectral sensitivities for the fully etched (thFBG) and attached fiber (IOF) geometry are comparable to empirical data.

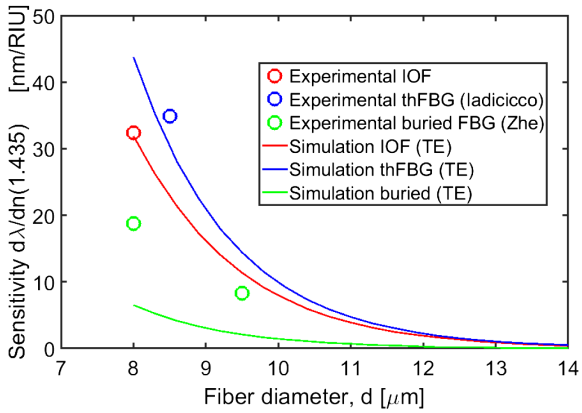


**Fig. 6.** Sensitivity comparison between the three geometries, showing the TE experimental data of IOF compared with the data for etched (Iadicicco [22]) and side-polished (Zhe [25]) structures, respectively.

The simulated sensitivity for the side access (buried FBG) regime underestimates sensitivity. However, this is believed to be due to the additional enhancement to the evanescent field brought about through the curved nature of the fiber when it is potted. From Fig. 6, it is observed that the spectral sensitivity of IOF sits between the side access and uniform access configurations. Practically, it was not possible to acquire sensitivities over 1.436, since the degradation of the spectral feature made interpretation difficult. This is believed to be a consequence of alignment issues of the Bragg grating, previously discussed. A misaligned grating would have a variable average core refractive index which, as observed in Fig. 4, has a large influence on sensitivity. Thus, at higher external refractive indices the grating quality deteriorates. Practically, this could be overcome through improving alignments or moving to alternative FBG writing approaches that do not use a small writing spot. As previously noted, the effective refractive index in air for the device is 1.45698. Furthermore, both the FHD and thermal oxide have indices of 1.4452. Therefore, guiding would still be expected at external refractive indices approaching 1.45. Through simulations, it can be inferred that sensitivities in this region would approach 224 nm/RIU. It is understood that thermal cross-sensitivity is a limiting factor for the device's current design. While this is minimal in a temperature-controlled laboratory, it would evidently become an issue in practical applications. There are several approaches for thermal referencing, the simplest being the use of a thermal reference grating that is locally placed and has a sufficient FHD coverage region of particular interest for automobile and aviation gasoline monitoring [23] as to be independent of external refractive index [10]. The implementation of this would require either localized etching along the fiber or localized FHD burial.

Quantification for the robustness of such a platform has no mechanical standard to draw. Therefore, robustness was measured through an attempted dislodgement of the fiber with a fingernail. In this qualification, the fingernail was passed firmly against the side of the fiber. Five attempted dislodgments were made after the fiber was subject to a 48 h soak in acetone, gasoline, and methanol, respectively, and a 300°C bake in air for 48 h (erasure of DUW Bragg gratings is known to occur at 400°C). After these tests, there was no notable physical degradation of the fiber or the optical signal; the fiber remained secured to the planar substrate. It is noted that recent progress in thermally regenerated Bragg gratings may offer an extension to the thermal range of FBGs in this layered configuration [26].

In conclusion, to the best of our knowledge, the first demonstration of an IOF refractometer has been made. Additionally, to the best of our knowledge, this marks the first demonstration of an IOF with exposed evanescent field. In addition, the consideration of optical interaction between separate attached fibers to create, for example, directional and cross-coupler components can be built upon, a concept that could achieve ultra-low loss integrated optics.

IOF was observed to have similar sensitivity compared to alternative geometries, but with the added advantage of being tolerant to environmental extremes. Future work will consider specific harsh environmental deployments for the platform.

**Funding.** Engineering and Physical Sciences Research Council (EPSRC) (EP/M013294/1); Higher Education Innovation Funding: University of Southampton Zepler Institute Research Collaboration Stimulus Fund.

## REFERENCES

1. S. J. Mihailov, Sensors **12**, 1898 (2012).
2. X. Qiao, Z. Shao, W. Bao, and Q. Rong, Sensors **17**, 429 (2017).
3. I. J. G. Sparrow, P. G. R. Smith, G. D. Emmerson, S. P. Watts, and C. Riziotis, J. Sens. **2009**, 607647 (2009).
4. S. G. Lynch, C. Holmes, S. A. Berry, C. James, A. Jantzen, T. I. Ferreiro, and P. G. R. Smith, Opt. Express **24**, 8391 (2016).
5. C. Holmes, J. C. Gates, and P. G. R. Smith, Opt. Express **22**, 32150 (2014).
6. C. Holmes, A. Jantzen, A. C. Gray, L. G. Carpenter, P. C. Gow, S. G. Lynch, J. C. Gates, and P. G. R. Smith, IEEE Sens. J. **17**, 6960 (2017).
7. A. D. Kersey, Opt. Fiber Technol. **2**, 291 (1996).
8. K. Schroeder, W. Ecke, R. Mueller, R. Willsch, and A. Andreev, Meas. Sci. Technol. **12**, 757 (2001).
9. D. Bhatta, A. A. Michel, M. Marti Villalba, G. D. Emmerson, I. J. G. Sparrow, E. A. Perkins, M. B. McDonnell, R. W. Ely, and G. A. Cartwright, Biosens. Bioelectron. **30**, 78 (2011).
10. C. Holmes, J. C. Gates, L. G. Carpenter, H. L. Rogers, R. M. Parker, P. A. Cooper, S. Chaotan, F. R. M. Adikan, C. B. E. Gawith, and P. G. R. Smith, Meas. Sci. Technol. **26**, 112001 (2015).
11. J. Homola, S. S. Yee, and G. Gauglitz, Sens. Actuators B **54**, 3 (1999).
12. S. Silva, P. Roriz, and O. Frazão, Photonics **1**, 516 (2014).
13. M. H. Frosz, A. Stefani, and O. Bang, Opt. Express **19**, 10471 (2011).
14. T. Han, Y. Liu, Z. Wang, B. Zou, B. Tai, and B. Liu, Opt. Lett. **35**, 2061 (2010).
15. W. Liang, Y. Huang, Y. Xu, R. K. Lee, and A. Yariv, Appl. Phys. Lett. **86**, 151122 (2005).
16. T. Erdogan and J. E. Sipe, J. Opt. Soc. Am. A **13**, 296 (1996).
17. C. Holmes, L. G. Carpenter, H. L. Rogers, I. J. G. Sparrow, J. C. Gates, and P. G. R. Smith, Opt. Express **19**, 12462 (2011).
18. K. R. Daly, C. Holmes, J. C. Gates, P. G. R. Smith, and G. D'Alessandro, IEEE Photon. J. **3**, 861 (2011).
19. S. W. James and R. P. Tatam, Meas. Sci. Technol. **14**, R49 (2003).
20. C. Holmes, K. R. Daly, I. J. G. Sparrow, J. C. Gates, G. D'Alessandro, and P. G. R. Smith, IEEE Photon. J. **3**, 777 (2011).
21. D. Xiaowei and Z. Ruifeng, Opt. Laser Technol. **42**, 214 (2010).
22. A. Iadicicco, A. Cusano, S. Campopiano, A. Cutolo, and M. Giordano, IEEE Photon. Technol. Lett. **16**, 1149 (2004).
23. H. W. Yarranton, J. C. Okafor, D. P. Ortiz, and F. G. A. Van Den Berg, Energy Fuels **29**, 5723 (2015).
24. F. P. Payne and J. P. R. Lacey, Opt. Quantum Electron. **26**, 977 (1994).
25. Z. Chen and L. Liu, Proc. SPIE **7157**, 71570J (2008).
26. A. Jantzen, R. H. S. Bannerman, S. A. Berry, J. C. Gates, P. C. Gow, L. J. Boyd, P. G. R. Smith, and C. Holmes, Opt. Lett. **42**, 3741 (2017).